Highly efficient conversion of superoxide to oxygen using hydrophilic carbon clusters

Errol L. G. Samuel[a,1], Daniela C. Marcano[a,b,1], Vladimir Berka[c,1], Brittany R. Bitner[d,e], Gang Wu[c], Austin Potter[a], Roderic H. Fabian[f,g], Robia G. Pautler[d,e], Thomas A. Kent[d,f,g,2], Ah-Lim Tsai[c,2], and James M. Tour[a,b,2]

[a]Department of Chemistry and [b]Smalley Institute for Nanoscale Science and Technology, Rice University, Houston, TX 77005; [c]Hematology, Internal Medicine, University of Texas Houston Medical School, Houston, TX 77030; [d]Interdepartmental Program in Translational Biology and Molecular Medicine and Departments of [e]Molecular Physiology and Biophysics and [f]Neurology, Baylor College of Medicine, Houston, TX 77030; and [g]Center for Translational Research in Inflammatory Diseases, Michael E. DeBakey Veterans Affairs Medical Center, Houston, TX 77030

Edited* by Robert F. Curl, Rice University, Houston, TX, and approved January 12, 2015 (received for review September 8, 2014)

Many diseases are associated with oxidative stress, which occurs when the production of reactive oxygen species (ROS) overwhelms the scavenging ability of an organism. Here, we evaluated the carbon nanoparticle antioxidant properties of poly(ethylene glycolated) hydrophilic carbon clusters (PEG-HCCs) by electron paramagnetic resonance (EPR) spectroscopy, oxygen electrode, and spectrophotometric assays. These carbon nanoparticles have 1 equivalent of stable radical and showed superoxide ($O_2^{\bullet-}$) dismutase-like properties yet were inert to nitric oxide ($NO^{\bullet}$) as well as peroxynitrite ($ONOO^-$). Thus, PEG-HCCs can act as selective antioxidants that do not require regeneration by enzymes. Our steady-state kinetic assay using KO_2 and direct freeze-trap EPR to follow its decay removed the rate-limiting substrate provision, thus enabling determination of the remarkable intrinsic turnover numbers of $O_2^{\bullet-}$ to O_2 by PEG-HCCs at >20,000 s^{-1}. The major products of this catalytic turnover are O_2 and H_2O_2, making the PEG-HCCs a biomimetic superoxide dismutase.

superoxide | antioxidant | carbon nanoparticles | hydrophilic carbon clusters | superoxide dismutase mimetic

Reactive oxygen species (ROS), such as superoxide ($O_2^{\bullet-}$), hydrogen peroxide (H_2O_2), organic peroxides, and hydroxyl radical ($^{\bullet}OH$), are a consequence of aerobic metabolism (1, 2). These ROS are necessary for the signaling pathways in biological processes (3, 4) such as cell migration, circadian rhythm, stem cell proliferation, and neurogenesis (5). In healthy systems, ROS are efficiently regulated by the defensive enzymes superoxide dismutase (SOD) and catalase, and by antioxidants such as glutathione, vitamin A, ascorbic acid, uric acid, hydroquinones, and vitamin E (6). When the production of ROS overwhelms the scavenging ability of the defense system, oxidative stress occurs, causing dysfunctions in cell metabolism (7–16).

In addition to ROS, reactive nitrogen species (RNS) such as nitric oxide ($NO^{\bullet}$), nitrogen dioxide, and dinitrogen trioxide can be found in all organisms. $NO^{\bullet}$ can act as an oxidizing or reducing agent depending on the environment (17), is more stable than other radicals (half-life 4–15 s) (18), and is synthesized in small amounts in vivo (17–22). $NO^{\bullet}$ is a potent vasodilator and has an important role in neurotransmission and cytoprotection (17, 18, 22, 23). Owing to its biological importance and the low concentration found normally in vivo, it is often important to avoid alteration of $NO^{\bullet}$ levels in biological systems to prevent aggravation of acute pathologies including ischemia and reperfusion.

One way to treat these detrimental pathologies is to supply antioxidant molecules or particles that renormalize the disturbed oxidative condition. We recently developed a biocompatible carbon nanoparticle, the poly(ethylene glycolated) hydrophilic carbon cluster (PEG-HCC), which has shown ability to scavenge oxyradicals and protect against oxyradical damage in rodent models and thus far has demonstrated no in vivo toxicity in laboratory rodents (24–27). The carbon cores of PEG-HCCs are ~3 nm wide and range from 30 to 40 nm long. Based on these data, we estimate that there are 2,000–5,000 sp^2 carbon atoms on each PEG-HCC core. We have demonstrated the efficacy of PEG-HCCs for normalizing in vivo $O_2^{\bullet-}$ in models of traumatic brain injury with concomitant hypotension. Simultaneously, we observed normalization in $NO^{\bullet}$ levels in these experiments (26, 27). A better understanding of these materials is necessary to potentially translate these therapeutic findings to the clinic.

In the present work, we evaluated antioxidant properties of PEG-HCCs. Using spin-trap EPR spectroscopy, we demonstrate that PEG-HCCs scavenge $O_2^{\bullet-}$ with high efficiency. X-ray photoelectron spectroscopy (XPS) indicates that covalent addition of ROS to the PEG-HCCs is not responsible for the observed activity. Direct measurement of $O_2^{\bullet-}$ concentration using freeze-trap EPR demonstrates that PEG-HCCs behave as catalysts, and measurements made with a Clark oxygen electrode during the reaction reveal that the rate of production of O_2 is above that expected due to self-dismutation of $O_2^{\bullet-}$ in water. An equivalent amount of H_2O_2 is also simultaneously produced. Finally, selectivity for ROS is confirmed using a hemoglobin and a pyrogallol red assay; PEG-HCCs are unreactive to both $NO^{\bullet}$ and $ONOO^-$. These results clarify the fundamental processes involved in the previously observed in vivo protection against oxygen damage (26, 27).

Significance

Mechanistic studies of nontoxic hydrophilic carbon cluster nanoparticles show that they are able to accomplish the direct conversion of superoxide to dioxygen and hydrogen peroxide. This is accomplished faster than in most single-active-site enzymes, and it is precisely what dioxygen-deficient tissue needs in the face of injury where reactive oxygen species, particularly superoxide, overwhelm the natural enzymes required to remove superoxide. We confirm here that the hydrophilic carbon clusters are unreactive toward nitric oxide radical, which is a potent vasodilator that also has an important role in neurotransmission and cytoprotection. The mechanistic results help to explain the preclinical efficacy of these carbon nanoparticles in mitigating the deleterious effects of superoxide on traumatized tissue.

Author contributions: D.C.M. designed research; E.L.G.S., D.C.M., V.B., B.R.B., G.W., A.P., R.H.F., and R.G.P. performed research; E.L.G.S., V.B., and G.W. contributed new reagents/analytic tools; T.A.K., A.-L.T., and J.M.T. directed research; E.L.G.S., V.B., B.R.B., R.H.F., R.G.P., T.A.K., A.-L.T., and J.M.T. analyzed data; and E.L.G.S., D.C.M., V.B., G.W., A.P., T.A.K., A.-L.T., and J.M.T. wrote the paper.

The authors declare no conflict of interest.

*This Direct Submission article had a prearranged editor.

[1]E.L.G.S., D.C.M., and V.B. contributed equally to this work.

[2]To whom correspondence may be addressed. Email: tkent@bcm.edu, Ah-Lim.Tsai@uth.tmc.edu, or tour@rice.edu.

This article contains supporting information online at www.pnas.org/lookup/suppl/doi:10.1073/pnas.1417047112/-/DCSupplemental.

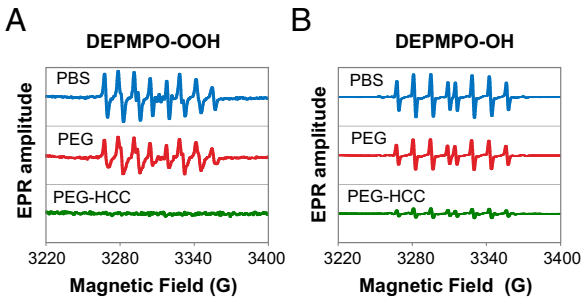

Fig. 1. Effect of PBS, PEG, and PEG-HCCs on $O_2^{\bullet-}$ and $^{\bullet}OH$ radicals. (*A*) EPR spectra obtained from the $O_2^{\bullet-}$ system or DEPMPO-OOH adduct at pH 7.4 and room temperature. Spectra were recorded after 70 s of the KO_2 addition. The PEG-HCCs spectrum was corrected by subtracting the signals of the PEG-HCCs alone. (*B*) EPR spectra obtained from the $^{\bullet}OH$ system or DEPMPO-OH. Spectra were recorded after 90 s of the H_2O_2 addition. The adduct stability was followed for 30 min. No correction was necessary for the $^{\bullet}OH$ scavenging experiments.

Results and Discussion

PEG-HCCs Scavenge $^{\bullet}OH$ and $O_2^{\bullet-}$. The scavenging capacity of PEG-HCCs was evaluated by EPR with the spin trap 5-(diethoxyphosphoryl)-5-methylpyrrole-N-oxide (DEPMPO). DEPMPO produces relatively stable paramagnetic adducts upon reaction with $^{\bullet}OH$ (3, 4, 28, 29) and $O_2^{\bullet-}$ (6, 29, 30) at room temperature (Fig. S1). We hypothesized that PEG-HCCs would scavenge $O_2^{\bullet-}$, resulting in a decreased EPR signal of the spin-adduct. EPR amplitudes of the DEPMPO-OOH and DEPMPO-OH adducts were lowest in the presence of PEG-HCCs (Fig. 1 *A* and *B*, respectively). $O_2^{\bullet-}$ was generated from KO_2 in DMSO/crown ether (31) and the $^{\bullet}OH$ radicals were generated in situ by the Fenton reaction (32). Simulations of the DEPMPO-OH and DEPMPO-OOH spectra confirmed the experimental identity of the spin-adducts (Fig. S1 and Table S1). Control experiments indicated that neither PEG nor PEG-HCCs destabilize the DEPMPO-OOH adduct. Note that the capture of $^{\bullet}OH$ by PEG-HCCs was also demonstrated, but the mechanistic relevance is unclear because its generation from H_2O_2 and metal would likely be far from the PEG-HCC reaction centers. Hence, kinetic data on $^{\bullet}OH$ are not highlighted here.

Further control experiments led to the detection of an intrinsic PEG-HCC radical possessing a symmetric spectrum centered at g = 2.0015 with an overall line width of 6 G and a half-saturation power at 0.74 mW at 115 K. We determined that for every 1 mol of PEG-HCCs there was 1 mol of unpaired electrons. This value was obtained based on five different batches of PEG-HCCs, including a batch that was 3 mo old, indicating that the nanoparticle-based radicals are very stable. Moreover, they are resistant to reductants such as ascorbate and dithionite and even inert to O_2 and $NO^{\bullet}$. Varying the pH from 2 to 12 did not alter the EPR lineshape of the radical. In contrast, only a very small intrinsic radical was found for two known antioxidant fullerene derivatives, C_3 (33) and C_{60}-serinol (34), at comparable concentration. This apparent correlation implies that this intrinsic radical may be linked to the activity of neutralizing $O_2^{\bullet-}$ and warrants further study.

To confirm the $O_2^{\bullet-}$ specificity of our spin-trap assay and to estimate PEG-HCC activity, the experiments were repeated in the presence of SOD1 (Cu/Zn-SOD), an enzyme that decomposes $O_2^{\bullet-}$ to H_2O_2 and O_2 (35–37). As expected, dismutation of $O_2^{\bullet-}$ was manifested by a decrease in the intensity of the 8-hyperfine line pattern of the adduct (Fig. 2). Comparison of the spectra clearly shows that PEG-HCCs have a quenching effect comparable to or better than that of 10 U/mL of SOD1. Based on the EPR amplitude of the DEPMPO spin trap, we calculated the antioxidant trapping (6) of $O_2^{\bullet-}$ by PEG-HCCs as 98% (Table S2).

Reaction of PEG-HCCs with $O_2^{\bullet-}$ Is Catalytic. Two mechanisms were considered for the observed $O_2^{\bullet-}$ antioxidant activity: (*i*) radical annihilation owing to the covalent bond formation between the radical and the graphitic domains of the PEG-HCCs and/or (*ii*) transformation of $O_2^{\bullet-}$ to O_2 by the PEG-HCCs. Because XPS only detected a slight oxygen increase (<10%, Fig. S2) in the PEG-HCCs after KO_2 treatment, covalent oxygen addition to the PEG-HCCs cannot be the main mechanism.

To test the transformation hypothesis, we established a manual freeze-trap EPR steady-state kinetic assay for $O_2^{\bullet-}$ consumption using KO_2 to provide excess $O_2^{\bullet-}$ and therefore shift the rate-limiting step to the intrinsic capability of PEG-HCCs in turning over $O_2^{\bullet-}$. This approach helped us to avoid the disadvantages of commonly used spin-trap EPR methods, which suffer from unfavorable trapping efficiencies and the loss of direct structural and kinetic information (17).

The typical EPR spectrum of 15-s freeze-trapped $O_2^{\bullet-}$ is characterized by the axial symmetry of its three principle g values (17, 38), and as Fig. 3 shows, the $O_2^{\bullet-}$ EPR signal decreased in the presence of PEG-HCCs. The rate of second-order self-dismutation of $O_2^{\bullet-}$ is very pH-sensitive and decreases exponentially from its pK_a (4.8) to pH 11 owing to increased charge repulsion between substrate molecules (39). Efforts to circumvent this at pH 8 by reducing [KO_2] to as low as 0.1 mM failed, because we could not freeze-trap any EPR-detectable radical. Therefore, to achieve sufficient and reliable concentrations of $O_2^{\bullet-}$ in solution, the quenching experiments are best carried out in 50 mM NaOH (pH 13).

As expected, the total spin concentration increased with the amount of added KO_2 (Fig. 4*A*). Consumption of $O_2^{\bullet-}$ was then calculated by subtracting these values from the control lacking PEG-HCCs and recalculated as turnover numbers (moles of consumed $O_2^{\bullet-}$ per moles of PEG-HCCs per second) with an average reaction time of 15 s (Fig. 4*B*). Our data showed saturation behavior of [$O_2^{\bullet-}$]. The maximum $O_2^{\bullet-}$ turnover amounted to a dramatic ~2.9 million (1.28 nM PEG-HCCs) and 1.1 million (6.4 nM PEG-HCCs) mol/15 s/mol, or 197,000 s^{-1} and 73,000 s^{-1}, respectively. In a puzzling twist, lower concentration of PEG-HCCs showed higher turnover efficiency. This could suggest that at higher concentrations there is more nanoparticle aggregation, lowering the overall turnover number. Although further detailed explanation for the [PEG-HCCs] dependency is not possible at this point, the extraordinary capacity of PEG-HCCs in quenching $O_2^{\bullet-}$ is underscored.

Our experiments suggest that PEG-HCCs behave as catalysts because the molar ratio of $O_2^{\bullet-}$ consumed to PEG-HCCs is far beyond the number of active sites, presuming the active sites are C atoms involved in sp^2 bonding on the PEG-HCCs in quantities determined previously (24, 25). Identical quenching experiments carried out using C_3 and C_{60}-serinol showed little catalytic activity

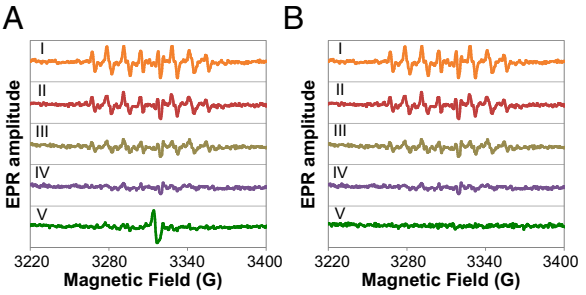

Fig. 2. (*A*) Uncorrected and (*B*) corrected EPR spectra of the samples treated with SOD vs. PEG-HCCs. The dismutation of the $O_2^{\bullet-}$ radicals is being catalyzed by SOD1 causes a signal drop. (*I*) SOD1 0.01 U/mL. (*II*) SOD1 0.1 U/mL. (*III*) SOD1 1 U/mL. (*IV*) SOD1 10 U/mL. (*V*) PEG-HCCs (0.07 mg/mL or 170.1 nM, which is the same concentration used in Fig. 1*A*). The spectrum in *B*, *V* was corrected by subtracting the EPR signal of the starting PEG-HCCs.

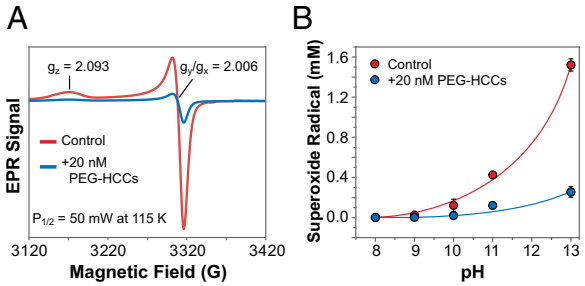

Fig. 3. Quenching of $O_2^{\bullet-}$ from KO_2 at varying pH. (*A*) EPR spectrum of $O_2^{\bullet-}$ in 50 mM NaOH in the presence and absence of PEG-HCCs. PEG-HCCs are able to quench $O_2^{\bullet-}$. (*B*) Quenching of $O_2^{\bullet-}$ at varying pH values; 20 mM KO_2 in DMSO was dissolved in different 50 mM buffers.

in quenching of $O_2^{\bullet-}$ (Fig. S3). Although the fullerenes have conjugated cores similar to those of the PEG-HCCs, there are clear structural differences. PEG-HCCs possess larger conjugated domains and bear a stoichiometric number of unpaired stable electrons, which could lower the activation energy for electron removal from $O_2^{\bullet-}$ to form O_2. Second, the C_{60} fullerenes have a highly curved structure, destabilizing a radical that prefers a planar conformation, whereas the PEG-HCCs are primarily planar and not tubular because there is no remaining radial breathing mode in their Raman spectra (24). It should be noted that although C_3 has been previously reported to have catalytic activity in the turnover of $O_2^{\bullet-}$ (40), the overall rate-limiting step in those experiments was substrate availability. By contrast, in our study, materials were tested in the presence of excess substrate and show that the activity of <10 nM PEG-HCCs is several orders higher than that of 20 μM C_3. Whether the presence of the intrinsic radical in the PEG-HCCs bears on the activity differences found here is unclear.

PEG-HCCs Are SOD Mimetics. Using a Clark-type oxygen electrode, we found that 4 nM PEG-HCCs substantially increased the rate of O_2 production but had no effect on the total amount of product (Fig. 5*A*). Subtracting the background O_2 formation rate (due to self-dismutation of $O_2^{\bullet-}$) resulted in a rate solely owing to the activity of PEG-HCCs, which showed typical Michaelis–Menten saturation kinetics (Fig. 5*B*); the $O_2^{\bullet-}$ turnover by PEG-HCCs in this experiment was estimated at 22,000 s^{-1}. This value is in the same range as that obtained from the EPR experiments and is closer to the 73,000 s^{-1} obtained with 6.4 nM PEG-HCCs. This >20,000 s^{-1} catalytic turnover number is higher than most single-active-site enzymes, suggesting that a PEG-HCC possesses multiple active sites.

Having confirmed O_2 generation, our attention turned to H_2O_2, the other potential major product of $O_2^{\bullet-}$ transformation. We investigated the production of H_2O_2 at either 15 s or 30 min of $O_2^{\bullet-}$ transformation in the presence and absence of PEG-HCCs in 50 mM NaOH. O_2 production was first measured for each sample at pH 13, after which the pH was lowered to ∼8 by a strong buffer and HRP was added along with Amplex Red. The reaction of Amplex Red and H_2O_2 in the presence of HRP produces the highly colored resofurin, which can be measured spectrophotometrically. Comparison of H_2O_2 production in the presence and absence of PEG-HCCs revealed the total amount of H_2O_2 to be the same (Fig. 5*C*). We consistently obtained a 1:1 molar correlation between O_2 and H_2O_2 produced in the same sample (Fig. 5*D*).

We then assessed the formation and stoichiometry of OH^- by measuring the pH change caused by the addition of KO_2 or KOH to 20 mM Hepes (pH 7.2) in the presence and absence of PEG-HCCs. The pH increase caused by added KO_2 was very close to that of the KOH control, and the presence of PEG-HCCs had no effect (Fig. S4). This outcome indicates that both self-dismutation and turnover by PEG-HCCs follow the same mechanism leading to OH^- formation, and the stoichiometry between $O_2^{\bullet-}$ and OH^- is 1:1. Together, the O_2, H_2O_2, and OH^- results suggest that PEG-HCCs catalyze $O_2^{\bullet-}$ conversion as a dismutation process:

$$\text{PEG-HCC}^{\bullet} + O_2^{\bullet-} \rightarrow \text{PEG-HCC}^{-} + O_2 \qquad [1]$$

$$\text{PEG-HCC}^{-} + O_2^{\bullet-} + 2\,H_2O \rightarrow \text{PEG-HCC}^{\bullet} + H_2O_2 + 2\,HO^{-}. \qquad [2]$$

Although there are product similarities to the model proposed by Ali et al. (40) for the C_{60} derivative C_3, our proposed mechanism is quite different. PEG-HCC can initially act as an electron acceptor (Eq. **1**) toward $O_2^{\bullet-}$ to form a highly delocalized, hence nonbasic, anion on the conjugated carbon framework, followed by acting as an electron donor to a second molecule of $O_2^{\bullet-}$ (Eq. **2**) with rapid capture of two protons from water to complete the catalytic cycle. If the initial reaction is not dependent on the intrinsic radical domain of the PEG-HCC, then the first step affords $\text{PEG-HCC}^{\bullet-}$, which returns to the neutral PEG-HCC in the second step. This latter motif permits the PEG-HCC to use multiple reaction centers, therefore better explaining the remarkably high turnover numbers that were recorded for conversion of $O_2^{\bullet-}$ to O_2. PEG-HCC anion stabilization can occur through the extended conjugated domain and through multiple neighboring carbonyl enolate-like interactions.

The similar pH shift observed with PEG-HCCs and the KOH control indicates that the abstraction of two protons from water to release OH^- (Eq. **2**) proceeds to completion. Although it may seem that there is a shortage of protons at pH 13, there are in fact >50 M water molecules, an abundant source. Moreover, the water molecules that provide the two protons in Eq. **2** are likely to be hydrogen-bonded with the transiently formed O_2^{2-} to facilitate proton transfer. Indeed, electron spin echo envelope modulation studies carried out by Narayana et al. (41) on frozen $O_2^{\bullet-}$ samples prepared in 5 M NaOH found that each $O_2^{\bullet-}$ is hydrogen-bonded to four polarized water molecules ready for proton transfer. The extremely high pK_a values for the two deprotonation steps of H_2O_2 to O_2^{2-} (12.7 and 25, respectively) (42) provide further driving force for rapidly establishing a new equilibrium after proton transfer. Importantly, this suggests that the PEG-HCC–catalyzed $O_2^{\bullet-}$ turnover can occur by similar mechanisms whether at pH 13 (50 mM NaOH) or at physiological pH.

To support this prediction, we compared the activity of PEG-HCCs with SOD at physiological pH by two methods: (*i*) competition with cytochrome *c* in trapping $O_2^{\bullet-}$ released in situ from the reaction of ferrous endothelial nitric oxide synthase oxygenase domain ($eNOS_{ox}$) with oxygen under uncoupling conditions (43, 44)

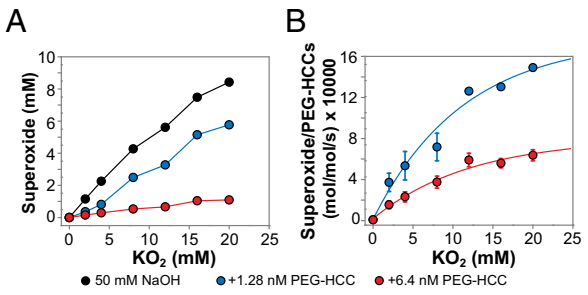

Fig. 4. KO_2 experiments in 50 mM NaOH. (*A*) $O_2^{\bullet-}$ total spin concentration based on double integration of obtained EPR spectra. For details, see *Methods*. (*B*) The turnover number (moles of superoxide per mole of PEG-HCCs per second) was calculated by subtracting the amount of remaining $O_2^{\bullet-}$ from the amount of $O_2^{\bullet-}$ in the control, dividing by the amount of PEG-HCCs and then by 15 s for the reaction time (the average time required for manually freeze-trapping each EPR sample).

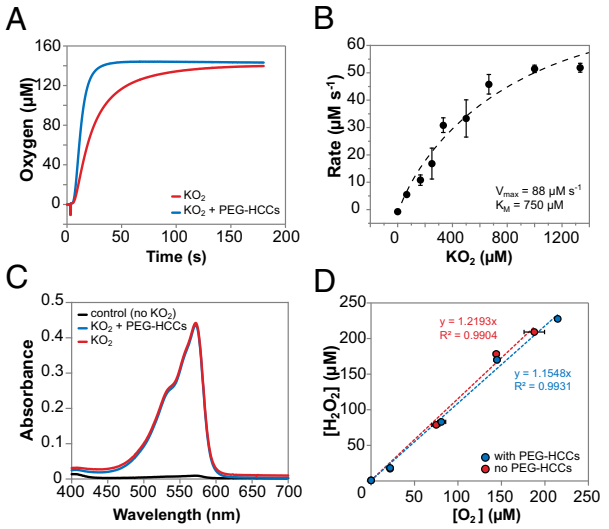

Fig. 5. Simultaneous O_2 and H_2O_2 production in the presence and absence of PEG-HCCs. (*A*) PEG-HCCs (4 nM) enhance the turnover of $O_2^{\bullet-}$ to O_2 but the total amount of O_2 generated does not change. (*B*) PEG-HCCs (4 nM) exhibited Michaelis–Menten kinetics with apparent K_m = 750 μM and V_{max} = 88 μM/s. The estimated turnover of $O_2^{\bullet-}$ by PEG-HCCs is 22,000 s^{-1}. (*C*) The amount of H_2O_2 produced in the presence and absence of PEG-HCCs is identical. (*D*) The ratio of $[O_2]$ to $[H_2O_2]$ produced by PEG-HCCs is 1:1.

and (*ii*) direct rapid-freeze quench (RFQ) EPR of $O_2^{\bullet-}$ produced from KO_2.

Both Cu/Zn SOD and PEG-HCCs showed dose-dependent competition with cytochrome *c*, yielding EC_{50} values of 2.5 nM and 254 nM, respectively (Fig. 6*A*). Although this seems to indicate that the catalytic turnover of $O_2^{\bullet-}$ by PEG-HCCs is two orders of magnitude less efficient, PEG-HCCs, but not SOD, also decreased the rate of cytochrome *c* reduction by approximately one order of magnitude (Fig. S5), indicating a complicated mechanism when using $eNOS_{ox}$ to generate $O_2^{\bullet-}$.

To avoid this problem, we used KO_2 to produce a continuous supply of $O_2^{\bullet-}$. Direct presentation of $O_2^{\bullet-}$ as KO_2 in the RFQ EPR kinetic measurements (Fig. 6*B*) showed that after a 20-ms reaction 2.2 mM KO_2 decayed to 0.52 ± 0.05, 0.39 ± 0.04, and 0.31 ± 0.02 mM (± SEM, n = 4) upon self-dismutation, SOD-catalyzed dismutation, and PEG-HCC–catalyzed dismutation, respectively. We thus observed 0.13 mM and 0.21 mM extra $O_2^{\bullet-}$ consumption upon addition of SOD and PEG-HCCs, corresponding to turnover numbers of 0.65×10^6 s^{-1} and 1.05×10^6 s^{-1}, respectively. On a molar basis, PEG-HCCs are as efficient at turning over $O_2^{\bullet-}$ as Cu/Zn SOD. Because the residual $O_2^{\bullet-}$ after 20-ms reaction was still at millimolar levels, steady-state kinetic requirements were met, and substrate provision was never a limiting factor. Using the results from the control sample, the second-order self-dismutation rate constant can be calculated as

$$\left(\frac{1}{0.52}-\frac{1}{2.2}\right)\times 9.25 = k \times 0.02 \text{ s},$$

where 9.25 is the dilution factor after unequal mixing with buffer in our rapid-freeze apparatus. k is calculated to be 6.8×10^5 $M^{-1}{\cdot}s^{-1}$, matching the theoretical rate constant for self-dismutation at pH 7.7 (45), indicating that our RFQ system operation was indeed optimal. The turnover number obtained at pH 7 is much higher than that obtained by manual mixing at pH 13, and this could be due to a real pH-dependent rate-limiting step. However, the pH 13 experiment employs a linear time-dependence treatment for a 15-s reaction that might deviate substantially from the exponential kinetics anticipated from PEG-HCC catalysis and thus could lead to an underestimation of the activity.

We also evaluated the antioxidant activity of PEG-HCCs by exposing them to $O_2^{\bullet-}$ generated during the turnover of hypoxanthine–xanthine oxidase (HX/XO), a system in which the rate-limiting step is the release of $O_2^{\bullet-}$, rather than in the antioxidant's intrinsic turnover efficiency. Here also, PEG-HCCs behaved as effective antioxidants, achieving inhibition equivalent to half of the positive control (IC_{50}), which was measured in the presence of a large excess of SOD. The IC_{50} of the PEG-HCCs was 0.20 ± 0.01 mg/mL or 486 ± 24 nM (Fig. 6*C*), higher than we observed for the $eNOS_{ox}$ system. Given the excellent in vitro and in vivo efficacy of PEG-HCCs (26, 27), the reduced activity in the presence of cytochrome *c* does not seem to have a significant effect clinically.

PEG-HCCs Are Inert to NO• and $ONOO^-$. Our previous in vitro endothelial culture and in vivo work on traumatic brain injury/hypotension models indicated no direct reaction between PEG-HCCs and NO• (27). Here we studied the antioxidant activity of PEG-HCCs against NO• using a hemoglobin assay to confirm the previous finding. The heme iron oxidation in oxyhemoglobin (HbO_2) by NO• is a fast (~10^8 $M^{-1}{\cdot}s^{-1}$) (17), quantitative, and irreversible reaction in which metHb and nitrate ion are produced (46, 47). In general, NO• can be indirectly determined by monitoring the production of metHb, estimated by the difference in absorbance at 401 and 411 nm with a difference extinction coefficient of 38 $mM^{-1}{\cdot}cm^{-1}$ (20, 21). If PEG-HCCs and HbO_2 react with the NO• radical at comparable rates, the PEG-HCCs would prevent the formation of metHb, resulting in a smaller absorbance difference. In the first experiments, HbO_2 and the PEG-HCCs were mixed and the reaction was initiated by addition of NO•. The conversion of HbO_2 to metHb is shown in Fig. S6. PEG-HCCs had no effect on this conversion, indicating that neither the absorbance of HbO_2 nor metHb was affected by the presence of the PEG-HCCs at these concentrations. The

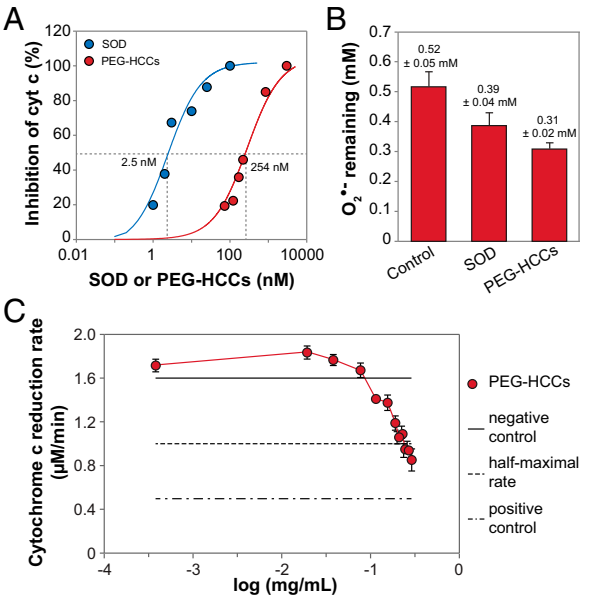

Fig. 6. Comparison of $O_2^{\bullet-}$ quenching activity of SOD and PEG-HCCs at physiological pH. (*A*) EC_{50} values of 2.5 nM for Cu/Zn SOD and of 254 nM for PEG-HCCs were determined using anaerobic stopped flow as a percentage of inhibition of reduction of cytochrome c^{3+}. Concentration of $eNOS_{ox}$ and cytochrome *c* was 10 μM and 15 μM, respectively. (*B*) KO_2 (2.2 mM) decayed to 0.52 ± 0.05, 0.39 ± 0.04, and 0.31 ± 0.02 mM upon self-dismutation, SOD-catalyzed dismutation, and PEG-HCCs–catalyzed dismutation, respectively; 20 nM each of SOD and PEG-HCCs was used. The error bars are SEM from four repeats. (*C*) The IC_{50} of the PEG-HCCs, as determined by the SOD-inhibitable reduction of ferricytochrome *c*, was 0.20 ± 0.01 mg/mL or 486 ± 24 nM.

difference between the control and the PEG-HCCs is only ~5%, which is less than the experimental error of ~10%. Hence, it can be concluded that either the PEG-HCCs are not quenching the $NO^{\bullet}$ radicals or that the reaction rate between the $NO^{\bullet}$ and the PEG-HCCs is much slower than the $NO^{\bullet}$ and HbO_2 reaction. To compare the rates of the reaction of PEG-HCCs with HbO_2 and PEG-HCCs with $NO^{\bullet}$, sequential stopped flow experiments were carried out (48). Either buffer (control) or PEG-HCCs were incubated with $NO^{\bullet}$ in a 1:1 ratio for 20 ms, 1 s, or 1 min, and this solution was then mixed with HbO_2 in a 1:1 ratio. There was no interaction between the PEG-HCCs and $NO^{\bullet}$ even after 1 min of preincubation. Furthermore, $NO^{\bullet}$ did not decay or decompose under these conditions. These results corroborate the in vitro and in vivo studies of the PEG-HCCs where no $NO^{\bullet}$ reaction was observed.

Because $NO^{\bullet}$ reacts rapidly with $O_2^{\bullet-}$ to form $ONOO^-$, the interaction between $ONOO^-$ and PEG-HCCs was also studied using the $ONOO^-$-induced quenching of the dye pyrogallol red (49, 50); if PEG-HCCs reacted with $ONOO^-$, then quenching of the dye would be inhibited. Ascorbic acid, caffeic acid, and Trolox all inhibited the quenching reaction in a manner consistent with reported results (48), but PEG-HCCs had no effect (Fig. S7). Bearing in mind that $NO^{\bullet}$ is constantly produced in vivo and is freely diffusible, production of $ONOO^-$ is more likely to occur in regions with a high local concentration of $O_2^{\bullet-}$. As was previously demonstrated, PEG-HCCs efficiently scavenge $O_2^{\bullet-}$, and this upstream scavenging effect will likely also decrease the amount of $ONOO^-$ produced in vivo.

In summary, we have demonstrated that PEG-HCCs quench $O_2^{\bullet-}$ catalytically. Nanomolar concentrations of PEG-HCCs are able to rapidly scavenge micromolar to millimolar concentrations of $O_2^{\bullet-}$. The turnover number of PEG-HCCs rivals that of Cu/Zn SOD at physiological pH. In addition, PEG-HCCs were inert to $NO^{\bullet}$, thereby potentially improving vascular homeostasis (51). Mechanistic studies based on our new saturation steady-state kinetic measurements enabled accurate determination of the turnover of $O_2^{\bullet-}$ by the PEG-HCCs. The proposed mechanism, derived from EPR and oxygen electrode experiments at pH 13, also applies at physiological pH. Taken together, these results demonstrate the efficacy of a carbon nanoparticle-based SOD mimetic.

Methods

For materials, see *Supporting Information*.

Spin-Trap $O_2^{\bullet-}$ Scavenging Assay. To a 2-mL microfuge tube was added potassium phosphate buffer (PBS, 50 mM, supplemented with 0.1 mM EDTA and 200 U/mL catalase); DEPMPO (20 mM); either PEG-HCCs (170 nM, Fig. S8 for MW estimation, or 0.07 mg/mL), PEG (14 μM or 0.07 mg/mL), or water; then KO_2 dissolved in DMSO (~3.0 mM). KO_2/DMSO was prepared following a modified reported procedure (31). Briefly, a 0.1 M stock solution of KO_2 in DMSO/crown ether was prepared according to the following procedure: 71.1 mg of KO_2 and 600 mg of crown ether were dissolved in 10 mL of DMSO. The mixture was stirred for 45–60 min until a clear pale yellow solution was obtained. The stock solution, stored at −70 °C, was stable for several weeks with no apparent decomposition.

During EPR experiments, time 0 was the time at which KO_2 was added to the aqueous reaction mixture. Subsequently, the mixture was transferred to a capillary tube, sealed with Critoseal, and placed in the EPR instrument. Owing to the time required for sample transfer to the capillary tube and then to the EPR cavity, the earliest that the EPR spectrum could be recorded was at 70 s. EPR measurements were recorded in a Bruker EMX spectrometer using the following parameters: center field, 3,315 G; sweep width, 200 G; microwave frequency, 9.3 GHz; microwave power, 40 mW; receiver gain, 6.32×10^5; modulation frequency, 100 kHz; modulation amplitude, 0.50 G; signal channel conversion, 163.8 ms; time constant, 327.7 ms; and sweep time, 167.8 s.

Direct EPR Detection of Radicals. PEG-HCCs were frozen in 5-mm EPR tubes using liquid nitrogen. The EPR spectra of the intrinsic radicals and a $CuSO_4$ (1 mM) standard solution were recorded at 115 K using the following parameters: 3,310 G as center field, 2,000 G sweep width, microwave frequency 9.3 GHz, microwave power 1 mW, receiver gain 7.1×10^3, modulation frequency 100 kHz, modulation amplitude 1.0 G. Because the copper standard and the PEG-HCC solutions were recorded under the same conditions, no corrections were necessary. The copper standard solution was supplemented with EDTA (10 mM) and $NaClO_4$ (100 mM) to make a homogeneous Cu-EDTA tetrahedral copper complex and uniform structure when frozen.

RFQ EPR Kinetic Measurements for $O_2^{\bullet-}$. Rapid-freeze quench EPR experiments were conducted using a System 1000 chemical/freeze quench apparatus (Update Instrument) with a Model 1019 syringe ram and a Model 715 controller. The ram velocity was 1.25 cm/s using a 0.008-inch nozzle to discharge the reaction solution. A low-temperature (125–130 K) isopentane bath was used for prechilling the assembly of a collecting funnel and EPR tube also filled with isopentane. Three syringes (two 2.1 mL, one 0.5 mL), two mixers, and two-push mixing syringe programs were used. In the control experiment, a 20 mM KO_2/DMSO solution was loaded into the 0.5-mL syringe and 0.1 M phosphate buffer, pH 7.7, was loaded in the 2.1-mL syringes. The first push mixed the solutions from the 2.1 mL syringes in mixer 1 while simultaneously filling the tubing to mixer 2. The second push mixed the buffer solution from mixer 1 with KO_2 from the 0.5-mL syringe in mixer 2. The final mixed sample was collected at 20 ms by rapid freeze quenching in prechilled isopentane. This mixing program achieves 9.25-fold dilution of KO_2 and < 9% DMSO in the final reaction mixture. In the experiments with SOD or PEG-HCCs, one of the 2.1-mL syringes was loaded with 20 nM SOD or PEG-HCCs in phosphate buffer. Reactions were conducted at room temperature (23 °C). Details of RFQ-EPR procedures have been described previously (52, 53). A packing factor of 0.45 was used for spin quantification of RFQ-EPR samples.

Steady-State Consumption of Superoxide. PEG-HCCs (1.28 nM and 6.4 nM) were mixed with increasing amounts of KO_2 dissolved in DMSO/18-crown-6 (5, 10, 15, 20, 25, or 50 μL) in medium [either water, N-Tris(hydroxymethyl)methyl-3-aminopropanesulfonic acid (TAPS), N-cyclohexyl-2-aminoethanesulfonic acid (CHES), N-cyclohexyl-3-aminopropanesulfonic acid (CAPS), or NaOH] for >15 s and then frozen in liquid N_2 to stop the reaction and preserve the remaining superoxide radical. EPR spectra were then recorded. To account for background dismutation of $O_2^{\bullet-}$, a sample lacking PEG-HCCs was measured and its EPR subtracted from sample spectra to obtain the amount of KO_2 decay catalyzed (or neutralized) by the PEG-HCCs. For comparative study, the assay was repeated using C_3 or C_{60}-serinol instead of PEG-HCCs.

Steady-State Oxygen Formation. Production of O_2 during the reaction of $O_2^{\bullet-}$ with PEG-HCCs was assayed polarographically at 24 °C with a YSI Model 5331 electrode (with a standard membrane) and a YSI Model 53 monitor. The reaction mixture (3.0 mL) contained 50 mM NaOH, 0.5 mM DETAPAC, and 4 nM PEG-HCCs. The reaction was started by addition of different amounts of KO_2. Activity of O_2 formation during the reaction was calculated from the initial slope.

Superoxide Turnover by Cytochrome *c* Reduction Using Burst Production of Superoxide from $eNOS_{ox}$. Recombinant human $eNOS_{ox}$ was expressed in *Escherichia coli* [tetrahydrobiopterin (BH_4) deficient] and purified as described previously (17, 44). Ferrous anaerobic $eNOS_{ox}$ (10 μM) in 0.1 M phosphate buffer with 0.1 M NaCl and 10% (vol/vol) glycerol (pH 7.7) was prepared by anaerobic titration with a minimal amount of dithionite and then mixed with oxygenated buffer containing 15 μM of ferric cytochrome *c* alone (as a control) or with different amounts of PEG-HCCs or SOD in an anaerobic stopped flow (SX-18MV; Applied Photophysics) (17). The amount of superoxide released by $eNOS_{ox}$ was determined by the cytochrome *c* reduction monitored at 550 nm ($21\ mM^{-1} \cdot cm^{-1}$) (54).

Cytochrome *c* Assay for $O_2^{\bullet-}$ from HX/XO. The $O_2^{\bullet-}$ scavenging efficiency was determined using the method described by Quick et al. (55). The assay was performed in a 96-well plate with the following conditions (four replicates): (*i*) a water blank (325 μL per well), (*ii*) solution without PEG-HCCs, (*iii*) solution with PEG-HCCs, and (*iv*) solution containing SOD (90 μL; 10,200 U/mL in PBS). After the addition of the HX/XO, a BIO-TEK Powerwave XS spectrophotometer (Molecular Devices) was used to read the plate at 550 nm every 45 s for 8 min. The reaction rate (OD per minute) was determined and then plotted as a function of the cytochrome *c* concentration ($\varepsilon_{550nm} = 21\ mM^{-1} \cdot cm^{-1}$) against the log of the concentration of the test compound. IC_{50} was determined using a nonlinear regression analysis (GraphPad Prism software, version 5.0).

Detection of H_2O_2 by Amplex Red Assay. Five microliters of KO_2 from a 0.1 M stock solution (prepared as previously described) was added to 95 μL of

5 mM NaOH and incubated for 15 s or 30 min in the presence and absence PEG-HCCs (5 μL of 0.9 mg/mL PEG-HCCs in 100 μL of 5 mM NaOH). Two microliters of the reaction mixture was added to 1 mL of 100 mM TAPS buffer (pH 8.2) containing 40 μM Amplex Red and 10 U/mL HRP. The optical spectrum of resofurin, the product of the reaction of Amplex Red with hydrogen peroxide, was measured using a diode array UV-visible spectrophotometer (8453; Hewlett Packard). The concentration of H_2O_2 was calculated using an extinction coefficient of 58 $mM^{-1}{\cdot}cm^{-1}$ at 570 nm.

pH Measurement of OH^- from KO_2. The pH change caused by KO_2, or KOH as a control, in the presence or absence of 0.6 μM PEG-HCCs, was measured by a pH meter (VWR Scientific with Orion 910500 combination pH electrode) after the addition of 1, 2, or 3 mM KO_2 or KOH to 5 mL of 20 mM Hepes buffer (pH 7.2). The stock solution of KO_2 was prepared as in the spin-trap $O_2^{\bullet-}$ scavenging assay.

ACKNOWLEDGMENTS. We thank Professor John S. Olson and Marian Fabian for the gift of human hemoglobin. We also thank Professor Lon Wilson (Rice University) for his C_{60}-serinol and Professor Douglas DeWitt (The University of Texas Medical Branch) for the C_3 samples. This work was funded by Mission Connect Mild Traumatic Brain Injury Consortium Grants W81XWH-08-2-0141 and W81XWH-08-2-0143, Alliance for NanoHealth Grant W81XWH-09-02-0139, and University of Texas Health Science Center through National Institutes of Health Grants HL095820 and NS084290.

1. Kulkarni RR, Virkar AD, D'mello P (2008) Antioxidant and antiinflammatory activity of Vitex negundo. *Indian J Pharm Sci* 70(6):838–840.
2. Bandyopadhyay U, Das D, Banerjee RK (1999) Reactive oxygen species: Oxidative damage and pathogenesis. *Curr Sci India* 77:658–666.
3. Živković J, et al. (2009) EPR Spin-trapping and spin-probing spectroscopy in assessing antioxidant properties: Example on extracts of catkin, leaves, and spiny burs of Castanea sativa. *Food Biophys* 4:123–133.
4. Spasojević I, et al. (2009) Relevance of the capacity of phosphorylated fructose to scavenge the hydroxyl radical. *Carbohydr Res* 344(1):80–84.
5. Dickinson BC, Chang CJ (2011) Chemistry and biology of reactive oxygen species in signaling or stress responses. *Nat Chem Biol* 7(8):504–511.
6. Jia Z, et al. (2008) EPR studies on the superoxide-scavenging capacity of the nutraceutical resveratrol. *Mol Cell Biochem* 313(1-2):187–194.
7. Sedelnikova OA, et al. (2010) Role of oxidatively induced DNA lesions in human pathogenesis. *Mutat Res* 704(1-3):152–159.
8. Valko M, et al. (2007) Free radicals and antioxidants in normal physiological functions and human disease. *Int J Biochem Cell Biol* 39(1):44–84.
9. Rocha M, Apostolova N, Hernandez-Mijares A, Herance R, Victor VM (2010) Oxidative stress and endothelial dysfunction in cardiovascular disease: Mitochondria-targeted therapeutics. *Curr Med Chem* 17(32):3827–3841.
10. Waris G, Ahsan H (2006) Reactive oxygen species: Role in the development of cancer and various chronic conditions. *J Carcinog* 5:14.
11. Phillips DC, Dias HK, Kitas GD, Griffiths HR (2010) Aberrant reactive oxygen and nitrogen species generation in rheumatoid arthritis (RA): Causes and consequences for immune function, cell survival, and therapeutic intervention. *Antioxid Redox Signal* 12(6):743–785.
12. Wiseman H, Halliwell B (1996) Damage to DNA by reactive oxygen and nitrogen species: Role in inflammatory disease and progression to cancer. *Biochem J* 313(Pt 1):17–29.
13. Rains JL, Jain SK (2011) Oxidative stress, insulin signaling, and diabetes. *Free Radic Biol Med* 50(5):567–575.
14. Kondratova AA, Kondratov RV (2012) The circadian clock and pathology of the ageing brain. *Nat Rev Neurosci* 13(5):325–335.
15. Uttara B, Singh AV, Zamboni P, Mahajan RT (2009) Oxidative stress and neurodegenerative diseases: A review of upstream and downstream antioxidant therapeutic options. *Curr Neuropharmacol* 7(1):65–74.
16. Barnham KJ, Masters CL, Bush AI (2004) Neurodegenerative diseases and oxidative stress. *Nat Rev Drug Discov* 3(3):205–214.
17. Berka V, Wang LH, Tsai A-L (2008) Oxygen-induced radical intermediates in the nNOS oxygenase domain regulated by L-arginine, tetrahydrobiopterin, and thiol. *Biochemistry* 47(1):405–420.
18. Archer S (1993) Measurement of nitric oxide in biological models. *FASEB J* 7(2): 349–360.
19. Yasmin S, Andrews SC, Moore GR, Le Brun NE (2011) A new role for heme, facilitating release of iron from the bacterioferritin iron biomineral. *J Biol Chem* 286(5):3473–3483.
20. Noak E, Kubitzek D, Kojda G (1992) Spectrophotometric determination of nitric oxide using hemoglobin. *Neuroprotocols* 1:133–139.
21. Kelm M, Dahmann R, Wink D, Feelisch M (1997) The nitric oxide/superoxide assay. Insights into the biological chemistry of the $NO/O^{\cdot 2-}$ interaction. *J Biol Chem* 272(15): 9922–9932.
22. Azarov I, et al. (2011) Mechanisms of slower nitric oxide uptake by red blood cells and other hemoglobin-containing vesicles. *J Biol Chem* 286(38):33567–33579.
23. Chung HT, Choi BM, Kwon YG, Kim YM (2008) Interactive relations between nitric oxide (NO) and carbon monoxide (CO): Heme oxygenase-1/CO pathway is a key modulator in NO-mediated antiapoptosis and anti-inflammation. *Methods Enzymol* 441:329–338.
24. Berlin JM, et al. (2010) Effective drug delivery, in vitro and in vivo, by carbon-based nanovectors noncovalently loaded with unmodified Paclitaxel. *ACS Nano* 4(8):4621–4636.
25. Bobadilla AD, Samuel ELG, Tour JM, Seminario JM (2013) Calculating the hydrodynamic volume of poly(ethylene oxylated) single-walled carbon nanotubes and hydrophilic carbon clusters. *J Phys Chem B* 117(1):343–354.
26. Marcano DC, et al. (2013) Design of poly(ethylene glycol)-functionalized hydrophilic carbon clusters for targeted therapy of cerebrovascular dysfunction in mild traumatic brain injury. *J Neurotrauma* 30(9):789–796.
27. Bitner BR, et al. (2012) Antioxidant carbon particles improve cerebrovascular dysfunction following traumatic brain injury. *ACS Nano* 6(9):8007–8014.
28. Spasojević I, Mojović M, Ignjatović A, Bacić G (2011) The role of EPR spectroscopy in studies of the oxidative status of biological systems and the antioxidative properties of various compounds. *J Serb Chem Soc* 76:647–677.
29. Livposky A (2009) EPR study of visible light-induced ROS generation by nanoparticles at ZnO. *J Phys Chem C* 113:15997–16001.
30. Frejaville C, et al. (1995) 5-(Diethoxyphosphoryl)-5-methyl-1-pyrroline N-oxide: A new efficient phosphorylated nitrone for the in vitro and in vivo spin trapping of oxygen-centered radicals. *J Med Chem* 38(2):258–265.
31. Bolojan L, Takacs IM, Miclaus V, Damian G (2012) An EPR study of superoide radicals from potassium superoxide solutions. *Appl Magn Reson* 42:333–341.
32. Chevion M, et al. (1993) Copper and iron are mobilized following myocardial ischemia: Possible predictive criteria for tissue injury. *Proc Natl Acad Sci USA* 90(3):1102–1106.
33. Bisaglia M, et al. (2000) C3-fullero-tris-methanodicarboxylic acid protects cerebellar granule cells from apoptosis. *J Neurochem* 74(3):1197–1204.
34. Wharton T, Wilson LJ (2002) Highly-iodinated fullerene as a contrast agent for X-ray imaging. *Bioorg Med Chem* 10(11):3545–3554.
35. Cohen G, Heikkila RE (1974) The generation of hydrogen peroxide, superoxide radical, and hydroxyl radical by 6-hydroxydopamine, dialuric acid, and related cytotoxic agents. *J Biol Chem* 249(8):2447–2452.
36. Liochev SI, Fridovich I (2007) The effects of superoxide dismutase on H2O2 formation. *Free Radic Biol Med* 42(10):1465–1469.
37. Keszler A, Kalyanaraman B, Hogg N (2003) Comparative investigation of superoxide trapping by cyclic nitrone spin traps: The use of singular value decomposition and multiple linear regression analysis. *Free Radic Biol Med* 35(9):1149–1157.
38. Knowles PF, Gibson JF, Pick FM, Bray RC (1969) Electron-spin-resonance evidence for enzymic reduction of oxygen to a free radical, the superoxide ion. *Biochem J* 111(1): 53–58.
39. Sheng Y, et al. (2014) Superoxide dismutases and superoxide reductases. *Chem Rev* 114(7):3854–3918.
40. Ali SS, et al. (2004) A biologically effective fullerene (C_{60}) derivative with superoxide dismutase mimetic properties. *Free Radic Biol Med* 37(8):1191–1202.
41. Narayana PA, Suryanarayana D, Kevan L (1982) Electron spin-echo studies of the solvation structure of superoxide ion (O2-) in water. *J Am Chem Soc* 104:3552–3555.
42. Petlicki J, van de Ven TGM (1998) The equilibrium between the oxidation of hydrogen peroxide by oxygen and the dismutation of peroxyl or superoxide radicals in aqueous solutions in contact with oxygen. *J Chem Soc, Faraday Trans* 94:2763–2767.
43. Xia Y, Tsai A-L, Berka V, Zweier JL (1998) Superoxide generation from endothelial nitric-oxide synthase. A Ca2+/calmodulin-dependent and tetrahydrobiopterin regulatory process. *J Biol Chem* 273(40):25804–25808.
44. Berka V, Wu G, Yeh H-C, Palmer G, Tsai A-L (2004) Three different oxygen-induced radical species in endothelial nitric-oxide synthase oxygenase domain under regulation by L-arginine and tetrahydrobiopterin. *J Biol Chem* 279(31):32243–32251.
45. Marklund S (1976) Spectrophotometric study of spontaneous disproportionation of superoxide anion radical and sensitive direct assay for superoxide dismutase. *J Biol Chem* 251(23):7504–7507.
46. Feelisch M, Noack EA (1987) Correlation between nitric oxide formation during degradation of organic nitrates and activation of guanylatecyclase. *Eur J Pharmacol* 139(1):19–30.
47. Lärfars G, Gyllenhammar H (1995) Measurement of methemoglobin formation from oxyhemoglobin. A real-time, continuous assay of nitric oxide release by human polymorphonuclear leukocytes. *J Immunol Methods* 184(1):53–62.
48. Tsai A-L, Berka V, Sharina I, Martin E (2011) Dynamic ligand exchange in soluble guanylyl cyclase (sGC): Implications for sGC regulation and desensitization. *J Biol Chem* 286(50):43182–43192.
49. Robaszkiewicz A, Bartosz G (2009) Estimation of antioxidant capacity against pathophysiologically relevant oxidants using Pyrogallol Red. *Biochem Biophys Res Commun* 390(3):659–661.
50. Papée HM, Petriconi GL (1964) Formation and decomposition of alkaline 'pernitrite'. *Nature* 204:142–144.
51. Gladwin MT, Kim-Shapiro DB (2008) The functional nitrite reductase activity of the heme-globins. *Blood* 112(7):2636–2647.
52. Tsai A-L, Berka V, Kulmacz RJ, Wu G, Palmer G (1998) An improved sample packing device for rapid freeze-trap electron paramagnetic resonance spectroscopy kinetic measurements. *Anal Biochem* 264(2):165–171.
53. Tsai Al, et al. (1999) Rapid kinetics of tyrosyl radical formation and heme redox state changes in prostaglandin H synthase-1 and -2. *J Biol Chem* 274(31):21695–21700.
54. Kuthan H, Ullrich V, Estabrook RW (1982) A quantitative test for superoxide radicals produced in biological systems. *Biochem J* 203(3):551–558.
55. Quick KL, Hardt JI, Dugan LL (2000) Rapid microplate assay for superoxide scavenging efficiency. *J Neurosci Methods* 97(2):139–144.